Science Advances
AAAS

advances.sciencemag.org/cgi/content/full/5/11/eaay0414/DC1

Supplementary Materials for

Tuning, optimization, and perovskite solar cell device integration of ultrathin poly(3,4-ethylene dioxythiophene) films via a single-step all-dry process

Meysam Heydari Gharahcheshmeh, Mohammad Mahdi Tavakoli, Edward F. Gleason, Maxwell T. Robinson, Jing Kong, Karen K. Gleason*

*Corresponding author. Email: kkg@mit.edu

Published 22 November 2019, *Sci. Adv.* **5**, eaay0414 (2019)
DOI: 10.1126/sciadv.aay0414

This PDF file includes:

Section S1. Methods and materials characterization

The oCVD process and Perovskite solar cell (PSC) device fabrication are described in the Materials and Methods section of the main text. The complementary details of methods and materials characterization are provided in this section.

The saturation pressure for the monomer (EDOT) and the oxidant ($VOCl_3$) at the temperature of interest were obtained using the Clausius–Clapeyron equation

$$P_2 = P_1 \cdot \exp\left(\frac{-\Delta H_{vap}}{R}\left(\frac{1}{T_2} - \frac{1}{T_1}\right)\right) \quad \text{(S1)}$$

where, ΔH_{vap} is the enthalpy of vaporization and R is the gas constant (8.3145 J mol^{-1} K^{-1}).

The Clausius-Clapeyron Equation allows estimating the vapor pressure at the temperature of interest if the vapor pressure at some temperature and enthalpy of vaporization are known. The saturation vapor pressure of EDOT as a function of temperature is shown in fig. S1A by knowing that the enthalpy of vaporization is 42.9 kJ/mol and the vapor pressure of EDOT at 25 °C is 0.278 Torr. The same procedure used for calculating the saturation vapor pressure of $VOCl_3$ by knowing that the enthalpy of vaporization is 36.78 kJ/mol and the vapor pressure of it at 20 °C is 13.8 Torr (fig. S1B). The information relates to the enthalpy of vaporization and the vapor pressure of each reactant at the specific temperature (ordinary close to the room temperature) was extracted form U.S national library of medicine that can be found at the PubChem website (https://pubchem.ncbi.nlm.nih.gov/). The values were also cross checked with the provided information by the vendor (Sigma-Aldrich).

The flow rate of EDOT and $VOCl_3$ are converted to the standard cubic centimeter per minute (SCCM) by degassing the oCVD reactor and calculating the volume of reactor and change of vapor pressure flow with respect to the time (dP/dt) based on the below equation

$$SCCM = 60 \times \left\{\left(\frac{V}{P}\right) \times \left(\frac{dP}{dt}\right) \times \frac{T_1}{T_2}\right\} - Reactor\ Leak\ Rate \quad \text{(S2)}$$

where, V is the volume of the oCVD reactor, P is the atmospheric pressure, dP/dt is the change of monomer or oxidant vapor pressure flow with respect to the time, T_1 is the reference condition for gas temperature (273.15 K), and T_2 is the temperature of inner oCVD reactor wall.

By using the basic knowledge of vacuum process, the flow rate of reactants can be converted to SCCM based on equation S2. The reactor volume was calculated based on the Boyle–Mariotte law ($V_2 = V_1(\frac{P_1}{P_2} - 1)$), where V_2 is the reactor volume, V_1 is the volume of big glass jar and portion of delivery line from glass jar to the valve (illustration is provided in Fig. 1), P_1 is atmospheric pressure, and P_2 is the reading pressure of baratron pressure transducer after opening the valve, while subtracting the base pressure (14 mTorr). The calculated reactor volume was 27696 cm^3. The temperature of inner reactor wall was around 100 °C, and the reactor leak rate was 1 mTorr/min (0.026 SCCM). The dP/dt was calculated after fully degassing the reactor and closing the throttle valve during 1 min and recording the pressure at the end of each 5-second interval. The dP/dt values were measured and calibrated before each run by adjusting the needle valve.

It should be noted that all PEDOT films were deposited at a fixed oCVD reactor pressure of 1 Torr. The amount of EDOT flow rate was kept constant at 12 SCCM during the deposition while the flow rate of $VOCl_3$ varied. The total flow rate into the oCVD reactor was kept at a fixed value of 30 SCCM at each growth temperature using Ar gas flow as a balancer of total flow rate. The detailed experimental conditions of flow rates into the oCVD reactor at different deposition temperature are inserted in table S1.

Materials characterization method:

Electrical conductivity measurement: The sheet resistance measurement was performed with a standard four-point probe method. For that purpose, the Jandal four-point probe (CYL-1.0-100-TC-100-RM3)

connected to Keithley 2000 and 2400 multimeters was used. Sheet resistivity is obtained by the four-point probe method as *(2)*

$$R_s = 4.5324\ \frac{V}{I} \tag{S3}$$

where R_s is a sheet resistance, V is the applied voltage, and I is the measured current.

The electrical conductivity, then obtained from the sheet resistance by

$$\sigma = \frac{1}{(R_s t)} \tag{S4}$$

where σ (S/cm) is electrical conductivity, R_s is sheet resistance, and t is the film thickness.

The film thickness is measured using a step-height profilometer (Veeco Dektak 150) and confirms with the Atomic Force Microscope (AFM, Veeco Dimension 3100).

Grazing incidence X-ray diffraction (GIXRD): The GIXRD measurements of oCVD PEDOT films grown on Si wafer were taken using a Rigaku Smart lab diffractometer operated at 45 kV and 200 mA with Cu-Kα radiation of λ=0.15418 nm. An X-ray beam probed the surface of the film at a fixed omega angle of 5° to reduce saturation by the primary beam. The analysis of the XRD data was conducted by Bruker software program Diffrac.Eva.

Scanning electron microscopy (SEM): The SEM imaging was carried out on Si micro-trenches coated with oCVD PEDOT using a cold field-emission gun Scanning electron microscope (FEG-SEM), JEOL 6700F.

X-ray photoelectron spectroscopy (XPS): The XPS analysis was performed on oCVD PEDOT films using a Surface Science Instruments SSX-100 with an operating pressure of approximately 2×10^{-9} Torr. The monochromatic Al Kα radiation with the photon energy of 1486.70 eV and diameter beam size of

1mm was used. The electron kinetic energy (KE) was determined using a hemispherical analyzer at the pass energy of 50 V for high resolution scans. The binding energy (BE) was determined by knowing the photon energy and KE values as: $BE = 1486.70 - \mathrm{KE}$. The atomic percentage (at. %) of elements was obtained from fitting XPS spectra using CasaXPS software.

Optical characteristics: The ultraviolet-visible-near infrared (UV-vis-NIR) spectroscopy was performed on PEDOT films deposited on microscope glass slides with 1 mm thickness using a Cary 7000 Universal Measurement Spectrometer equipped with an integrating sphere detector.

Perovskite device characterization method: The PSCs were characterized using a digital source meter (Keithley model 2400, USA) and a sun simulator (a 450 W xenon lamp (Oriel, USA)). The light was filtered by a Schott K113 Tempax (Präzisions Glas & Optik GmbH, Germany) to simulate the AM1.5G standard condition. The active area of each device was 0.054 cm^2. The devices were measured with a voltage scan rate of 10 mV/s. The external quantum efficiency of the devices was measured using a commercial apparatus (Arkeo-Ariadne, Cicci Research s.r.l.) with a 300 Watts Xenon lamp. Notable, the value for hysteresis index was calculated from the following equation

$$\mathrm{HI} = ((\mathrm{PCE}_{\mathrm{backward}} - \mathrm{PCE}_{\mathrm{forward}})/\mathrm{PCE}_{\mathrm{backward}}) \times 100 \quad \text{(S5)}$$

The solar spectrum of sunlight (AM1.5) is usually in the unit of power per area per wavelength (Wm^{-2} nm^{-1}). The short circuit current density (J_{sc}) is calculated based on the photon flow at a certain wavelength (λ) with EQE at that wavelength and zero bias

$$J_{sc} = q \int F(\lambda).EQE(\lambda, 0).d\lambda \quad \text{(S6)}$$

where q is the unit of charge, and $F(\lambda)$ is the photon flow at a wavelength of λ.

We need to calculate EQE of a device because: 1) an incoming photon does not always contribute a quantum of charge, 2) photons in some wavelengths may be weakly absorbed, and 3) solar cell device may not deliver one quantum of charge for every absorbed photon.

Section S2. Normalized integrated intensity based on LP factor, investigation of crystallite size, and lattice parameter

The effects of growth temperature and oxidant saturation ratio on the structural properties of oCVD PEDOT films were investigated using Grazing Incidence X-ray Diffraction (GIXRD). The systematic GIXRD investigation of PEDOT films grown at different deposition temperature and oxidant saturation ratio is provided in fig. S3. The GIXRD patterns indicate that the oCVD deposition parameters drastically influence the degree of crystallinity and π-π interchain stacking orientation of the PEDOT films. As can be noted all PEDOT films grown at the deposition temperature of 140 °C exhibit pure face-on orientation. There is an evolution of diffraction peak at the scattering angle of 2θ~12.8°, which is an indication of (200) peak (edge-on orientation) in PEDOT film grown at the deposition temperature of 110 °C and $VOCl_3$ saturation ratio of 1260 ppm. Also, there is another faint evolution of diffraction peak with increase in oxidant saturation ratio at the scattering angle of 2θ~19.2° in that sample and it can be indexed as the same type of edge-on orientation (h00), where h=3.

The normalized integrated peak intensity information for PEDOT films grown at different process parameters is inserted in table S2. The Lorentz Polarization (LP) factor used to compare the integrated peak intensity ratio of face-on and edge-on orientation. The Lorentz (L) correction factor is related to the geometry of the diffraction mode and is described as

$$L = \frac{1}{Cos(\theta).Sin^2(\theta)} \quad \text{(S7)}$$

The Polarization (P) factor is related to the assumption that the non-polarized X-ray beam may become partially polarized on reflection from the substrate surface and is described as

$$P = \frac{1+Cos^2(2\theta)}{2} \quad \text{(S8)}$$

The combination of Lorentz and Polarization correction factors is known as the Lorentz-polarization (LP) factor and controls X-ray intensity with respect to diffraction angle and is described as *(26)*

$$LP(\theta) = \frac{1+Cos^2(2\theta)}{Cos(\theta).Sin^2(\theta)} \quad \text{(S9)}$$

The LP factor for the diffraction angle of 2θ~6.4° (edge-on orientation) is much bigger than its counterpart for the diffraction angle of 2θ~25.5° (face-on orientation). The LP factor at each peak position is calculated and inserted in table S2. After calculating the LP factor for both edge-on and face-on orientation, the normalized Edge-on Integrated Intensity is converted to equivalent face-on integrated peak intensity based on:

$$\text{Normalized Edge-on Integrated Intensity} \times (L_p \text{ (Face-on)}/\ L_p \text{ (Edge-on)}) \quad \text{(S10)}$$

The resulted information is inserted in table S2. The percentage of preferential orientation was calculated based on the normalized integrated peak intensities of related face-on and edge-on orientations. The schematic illustration of preferred orientation after considering the LP factor as described above is exhibited in Fig. 2D.

The crystallite size is calculated from the full width at half maximum (FWHM) of the diffraction peaks using the Scherrer equation *(38)*

$$D = \frac{s\,\lambda}{\beta \cos\theta} \quad \text{(S11)}$$

where D, s, λ, β, θ are the average crystallite size, dimensionless shape factor (typically taken as 0.9), wavelength of the incident X-ray beam, FWHM of a diffraction peak, and half of the diffraction angle (2θ), respectively.

It was noted that the peak position of PEDOT (020) reflection shifts toward the lower diffraction angles by an increase in oxidant saturation ratio (fig. S3C and fig. S3D). Such a shift in a peak position toward lower diffraction angle is an indication of expansion in the distance between (020) planes.

The b-axis lattice parameter corresponds to the distance between π-π interchain stacking, while the a-axis lattice parameter refers to the distance of π-π stacking side to side as illustrated in Fig. 2B and Fig. 2C. The obtained values of b-axis and a-axis lattice parameters in PEDOT films grown at the different process parameters are inserted in table S5.

Section S3. Hopping probability by Miller-Abrahams model

In addition to interchain coupling through the decrease of b-axis lattice parameter, the increase of electrical conductivity can also be correlated to lowering b-axis lattice parameter in the hopping mechanism, which is described by the Miller-Abrahams. This mechanism is valid for weak electron-phonon coupling and low temperatures. In this mechanism, the probability of polarons hopping from a localized state (i) with energy E_i to an empty state (j) with energy E_j is expressed as tunneling factor ($\frac{-2L}{\xi}$) and Boltzmann factor ($-\frac{\Delta E_{ij}}{k_B T}$) as *(45)*

$$P_{ij} \propto exp\left\{\frac{-2L}{\xi_0} - \frac{\Delta E_{ij}}{k_B T}\right\} \quad \text{(S12)}$$

where P_{ij} is the hopping probability from state i to j, L is the hopping distance, ξ_0 is the localization length at zero magnetic field, $\Delta E_{ij} = E_j - E_i$ is the difference in energy between the localized state and empty state, k_B is the Boltzmann constant, T is the absolute temperature.

It is noteworthy to mention that the probability of polarons hopping to upward and downward energy levels is the same, unlike the IMT model. The local morphology and interchain orientation and distance are highly dependent on the synthesis process.

Section S4. Optical bandgap (E_g) and Urbach energy (E_U) investigation

The absorption spectra of PEDOT films (fig. S6) were obtained after subtracting the absorption spectra of substrates (microscope glass slides). The reflectance values of PEDOT films obtained from integrating sphere detector were in the range of ~0.5%. The optical band gap (E_g) is determined from the absorption spectra (fig. S6) using the Tauc relation *(48)*

$$\alpha h\vartheta = A(h\nu - E_g)^n \qquad (10)$$

where α is absorption coefficient, $h\vartheta$ is photon energy, A is constant, E_g is optical band gap, and n is type of transition (here n =1/2 for direct transition).

The procedure of extracting E_g is to plot $(\alpha h\vartheta)^2$ versus $h\vartheta$ and then extrapolation of the straight line to $(\alpha h\nu)^2 = 0$. One can notice that at $\alpha = 0$, $h\vartheta = E_g$. The value of ν when absorption coefficient (α) is zero is c/λ_{ab}. Therefore the optical band gap can be calculate from

$$E_g = hc/\lambda_{ab} \qquad (S13)$$

where h is Planck constant, and c is speed of light, and λ_{ab} is absorption wavelength.

The intersection of a line tangent to the absorption edge spectrum with the x-axis indicates the value of the absorption wavelength as is shown in fig. S6.

Fig. S7 displays the $\ln(\alpha)$ as a function of incident photon energy ($h\vartheta$) for PEDOT films grown at the deposition temperature of 140 °C and different oxidant saturation ratio. The α values, in the unit of 1/cm, were obtained by knowing the absorbance values and path length (here, is the film thickness) as: $\alpha = \frac{absorbance}{film\ thickness}$. The incident photon energy was determined from $E = h\vartheta = hc/\lambda$, where h is the Planck constant (6.63×10^{-34} J.s), c is the speed of light (3×10^{8} m/s), and λ is wavelength. The absorption coefficient beyond the optical band gap edge is fitted with the linear equation to determine the slope, the inverse of which gives the Urbach energy (E_u) based on the following equation

$$\ln \alpha = \ln \alpha_0 + \left(\frac{h\vartheta}{E_u}\right) \tag{S14}$$

Table S1. The deposition parameters used in the growth of oCVD PEDOT films. Experimental details relate to the monomer (EDOT) and oxidant ($VOCl_3$) flow rates into the oCVD reactor and corresponding vapor saturation ratio values.

Deposition Temperature (°C)	**EDOT Flow Rate (SCCM)**	**$VOCl_3$ Flow Rate (SCCM)**	**Ar Flow Rate (SCCM)**	**Total Flow Rate (SCCM)**	**oCVD Reactor Pressure (Torr)**	**EDOT P/P_{sat} (ppm)**	**$VOCl_3$ P/P_{sat} (ppm)**
110	12	4.5	13.5	30	1	30000	310
110	12	6	12	30	1	30000	420
110	12	7.5	10.5	30	1	30000	520
110	12	9	9	30	1	30000	630
110	12	12	6	30	1	30000	840
110	12	15	3	30	1	30000	1050
110	12	18	0	30	1	30000	1260
140	12	4.5	13.5	30	1	10000	140
140	12	6	12	30	1	10000	180
140	12	7.5	10.5	30	1	10000	230
140	12	9	9	30	1	10000	270
140	12	12	6	30	1	10000	360
140	12	13.5	4.5	30	1	10000	410
140	12	15	3	30	1	10000	450
140	12	16.5	1.5	30	1	10000	500
140	12	18	0	30	1	10000	540

Table S2. The normalized integrated peak intensity of oCVD PEDOT films. The normalized peak intensity information and % preferential edge-on and face-on orientations by considering the Lorentz-polarization (LP) factor.

Deposition Temperature (°C)	$VOCl_3$ P/P_{sat} (ppm)	Normalized Face-on Integrated Intensity*	Normalized Edge-on Integrated Intensity**	Converted Edge-on Intensity (Normalized Edge-on Integrated Intensity × (L_p (Face-on)/ L_p (Edge-on))****	% Preferred Edge-on Orientation	% Preferred Face-on Orientation
110	310	0.098	0	0	0	100
110	420	0.172	0	0	0	100
110	520	0.267	0	0	0	100
110	630	0.261	0.035	0.002	0.766	99.234
110	840	0.288	0.045	0.003	1.042	98.958
110	1050	0.175	0.244	0.015	8.571	91.429
110	1260	0.173	0.453***	0.027	15.607	84.393
140	140	0.023	0	0	0	100
140	180	0.025	0	0	0	100
140	230	0.053	0	0	0	100
140	270	0.055	0	0	0	100
140	360	0.105	0	0	0	100
140	410	0.128	0	0	0	100
140	450	0.107	0	0	0	100
140	500	0.134	0	0	0	100
140	540	0.170	0	0	0	100

*The reported values are attributed to the integrated peak intensity of (020)

**The reported values are attributed to the integrated peak intensity of (100)

***The reported value is the sum of normalized edge-on integrated intensity for diffraction peaks of (100), (200), and (300).

****L_p; Lorentz polarization (L_p) factor which is defined as $L_p(\theta) = \frac{1+\mathrm{Cos}^2(2\theta)}{\mathrm{Sin}^2(\theta)\,\mathrm{Cos}\,(\theta)}$

Table S3. The XPS elemental analysis of PEDOT films. The atomic percentage (at. %) of as-grown oCVD PEDOT films at the deposition temperature of 140 °C and different oxidant saturation values.

$VOCl_3$ P/P_{sat} (ppm)	S %	Cl %	C %	O %	V %
140	14.38	4.52	63.56	17.54	0
360	14.16	6.48	61.58	17.72	0.06
540	11.94	8.22	59.98	19.74	0.13

Table S4. The crystallite domain size in PEDOT films. The face-on and edge-on crystalline sizes in films grown at different deposition temperature and oxidant saturation ratio.

Deposition Temperature (°C)	$VOCl_3$ P/P_{sat} (ppm)	Extracted (100) Peak Position (Degree)	Extracted (020) Peak Position (Degree)	FWHM of (100) Peak (Degree)	FWHM of (020) Peak (Degree)	PEDOT crystallite Size in Edge-on Orientation (nm)	PEDOT crystallite Size in Face-on Orientation (nm)
110	310	-	25.4905	-	2.8161	-	3.104
110	420	-	25.4712	-	2.7303	-	3.208
110	520	-	25.4778	-	2.6137	-	3.363
110	630	6.4003	25.4420	1.2162	2.72592	7.767	3.214
110	840	6.3987	25.4493	1.2618	2.6079	7.436	3.371
110	1050	6.3602	25.3520	1.6087	2.7853	5.615	3.140
110	1260	6.3681	25.3393	1.7220	2.7921	5.199	3.131
140	140	-	25.5457	-	2.8074	-	3.114
140	180	-	25.5132	-	2.8303	-	3.087
140	230	-	25.5001	-	2.8266	-	3.091
140	270	-	25.4978	-	2.7421	-	3.194
140	360	-	25.4587	-	2.6923	-	3.257
140	410	-	25.4654	-	2.6362	-	3.332
140	450	-	25.4354	-	2.7505	-	3.183
140	500	-	25.4032	-	2.8014	-	3.121
140	540	-	25.3987	-	2.5357	-	3.474

Table S5. The *a*-axis and *b*-axis lattice parameter information of PEDOT films. The extracted lattice parameters of films grown at the different deposition temperature and oxidant saturation ratio.

Deposition Temperature (°C)	$VOCl_3$ P/P_{sat} (ppm)	Extracted (100) Peak Position (Degree)	d-spacing between (100) planes	Extracted (020) Peak Position (Degree)	d-spacing between (020) planes	a-axis Lattice Parameter (A)*	b-axis Lattice Parameter (A)**
110	310	-	-	25.4905	3.492	-	6.984
110	420	-	-	25.4712	3.494	-	6.988
110	520	-	-	25.4778	3.493	-	6.986
110	630	6.4003	13.799	25.4420	3.498	13.799	6.996
110	840	6.3987	13.802	25.4493	3.497	13.802	6.994
110	1050	6.3602	13.886	25.3520	3.510	13.886	7.020
110	1260	6.3681	13.868	25.3393	3.512	13.868	7.024
140	140	-	-	25.5457	3.487	-	6.974
140	180	-	-	25.5132	3.489	-	6.978
140	230	-	-	25.5001	3.490	-	6.980
140	270	-	-	25.4978	3.491	-	6.982
140	360	-	-	25.4587	3.496	-	6.992
140	410	-	-	25.4654	3.495	-	6.990
140	450	-	-	25.4354	3.499	-	6.998
140	500	-	-	25.4032	3.503	-	7.006
140	540	-	-	25.3987	3.504	-	7.008

*a-axis lattice parameter = d-spacing between (100) planes.

**b-axis lattice parameter = 2× d-spacing between (020) planes.

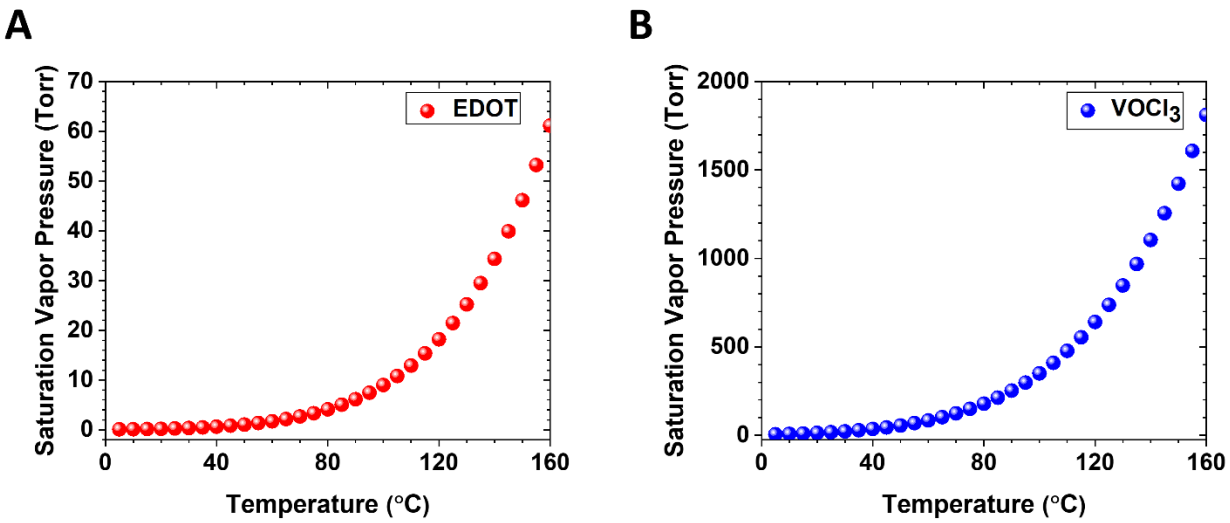

Fig. S1. Saturation vapor pressure of monomer and oxidant at different temperatures. The calculated saturation vapor pressure of (**A**) EDOT as a monomer reactant, and (**B**) $VOCl_3$ as an oxidant reactant at the different temperatures. The saturation vapor pressure was obtained based on the Clausius-Clapeyron equation.

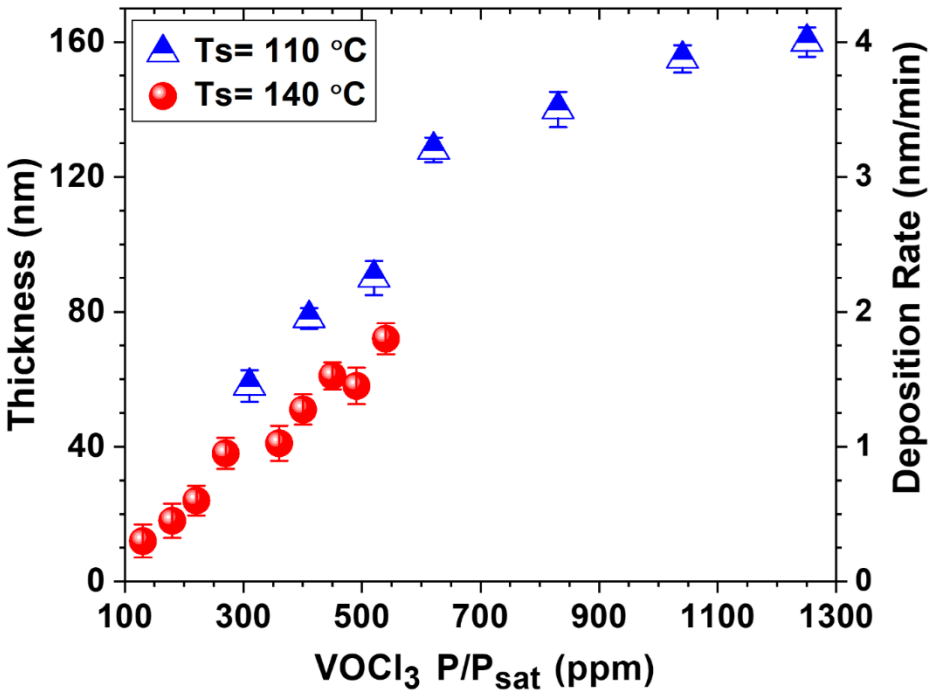

Fig. S2. Thickness and deposition rate of PEDOT films as a function of process parameters. The effect of oxidant saturation ratio and deposition temperature on the thickness and deposition rate of PEDOT films. The saturation ratio of EDOT was kept fixed at 0.03 and 0.01 at the deposition temperature of 110 °C and 140 °C, respectively.

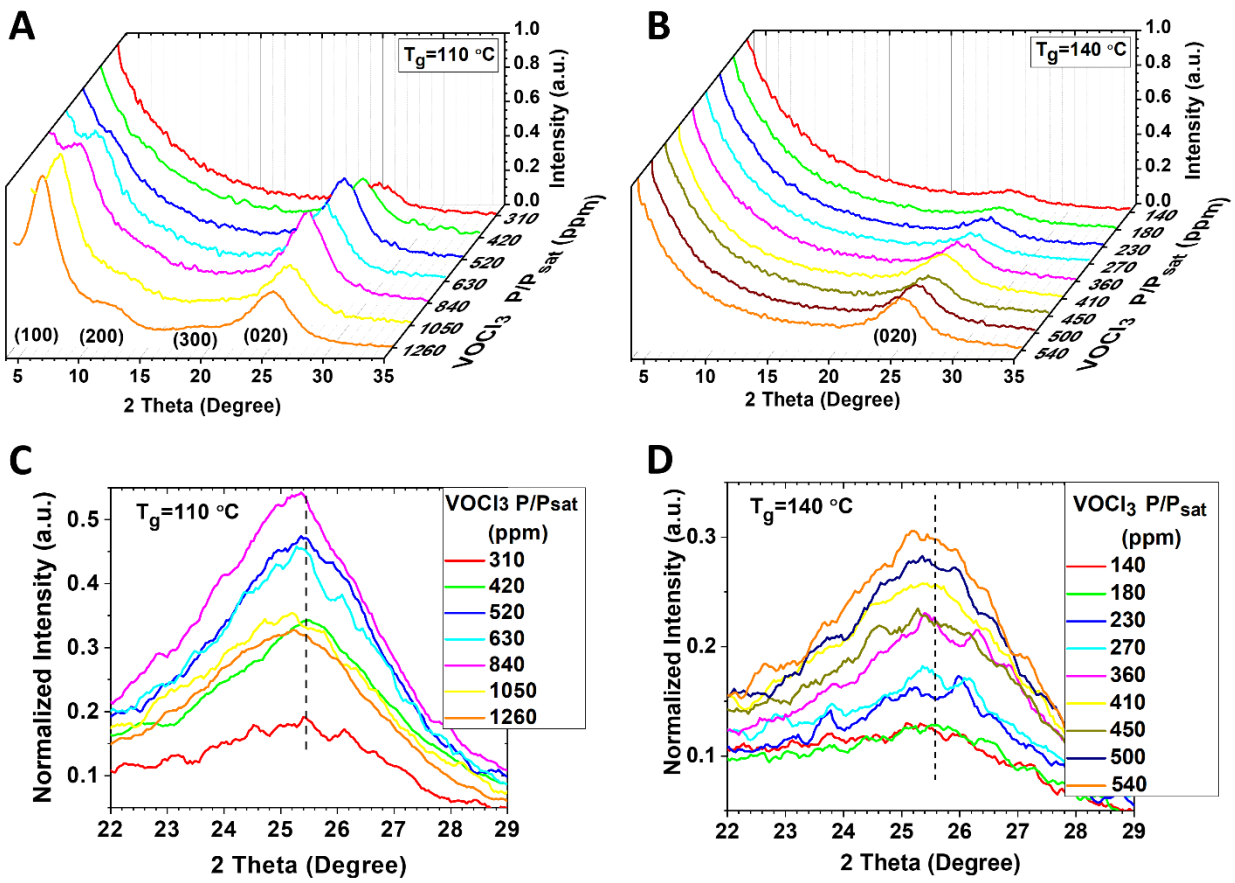

Fig. S3. Effect of process parameters on the crystalline orientation of PEDOT films. The systematic investigation of the out-of-plane GIXRD θ–2θ diffraction patterns PEDOT films grown with different $VOCl_3$ saturation ratio at the deposition temperature of (**A**) 110 °C, and (**B**) 140 °C. The XRD patterns with high magnification around the PEDOT (020) peak in films grown with different oxidant saturation ratio at the deposition temperature of (**C**) 110 °C, and (**D**) 140 °C. The shift in peak position toward lower diffraction angles can be noticed by increasing the oxidant saturation ratio.

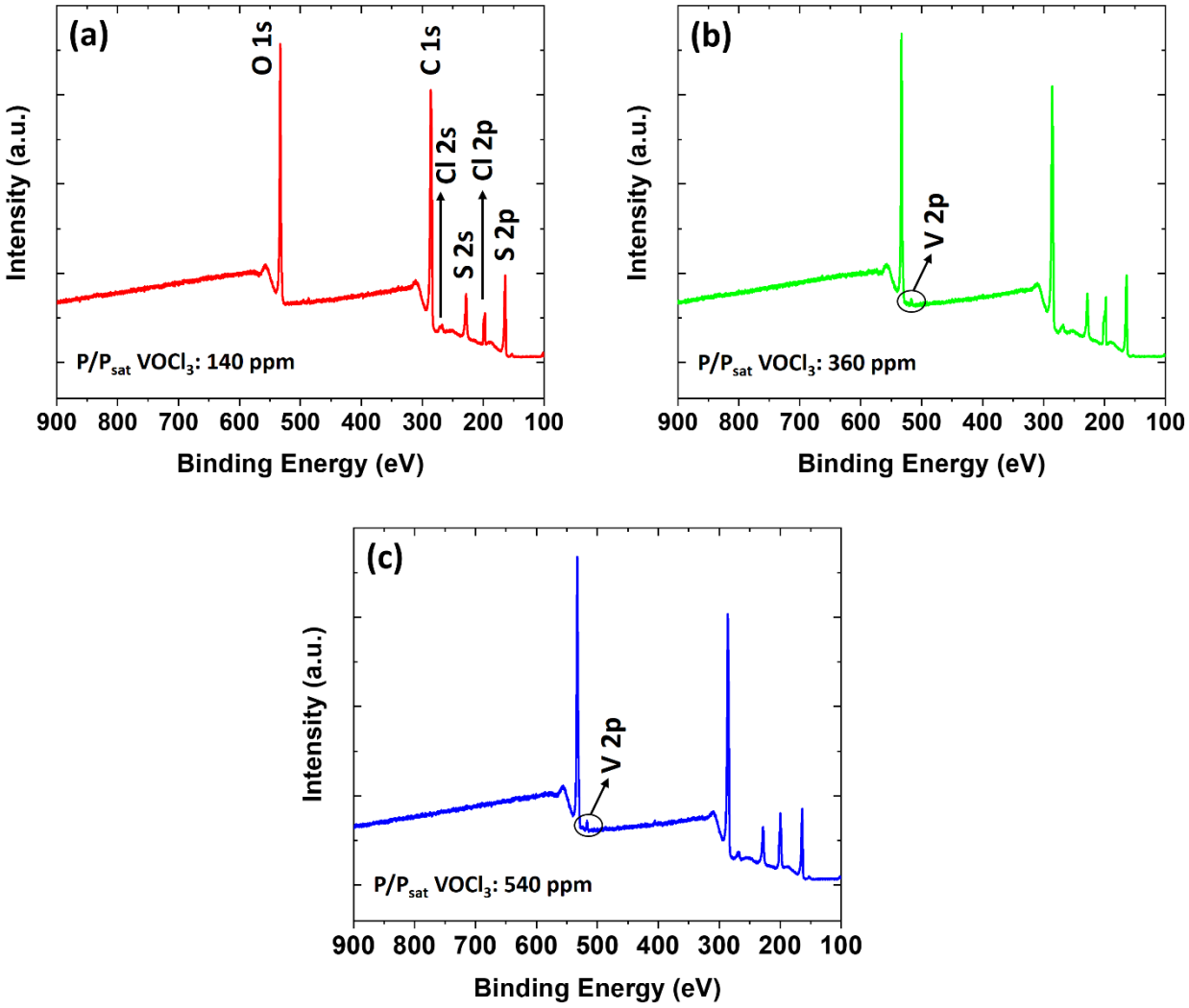

Fig. S4. The XPS analysis of PEDOT films. Survey scan for as-grown oCVD PEDOT films at the deposition temperature of 140 °C with different OSR of (a) 140 ppm, (b) 360 ppm, and (c) 540 ppm. The absent of oxidant by-products was observed in PEDOT films, and the maximum at. % of vanadium was 0.13% in film grown at the OSR value of 540 ppm. The vanadium at. % in films grown at the OSR value of 140 and 360 ppm was 0.00% and 0.06%, respectively.

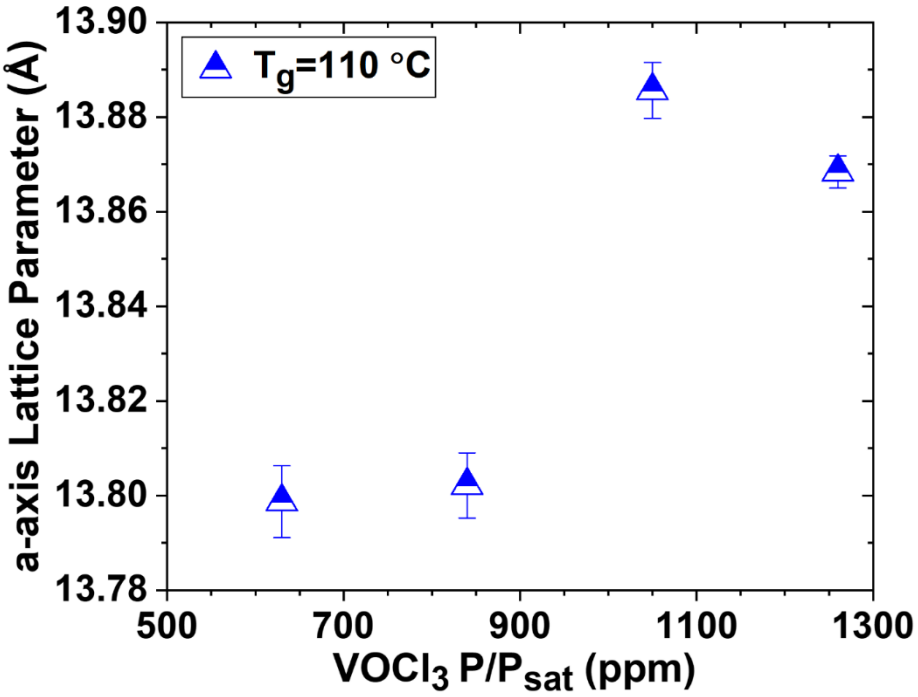

Fig. S5. The effect of OSR on the *a*-axis lattice parameter of PEDOT films. The a-axis lattice parameter as a function of oxidant saturation ratio in PEDOT films grown at the deposition temperature of 110 °C.

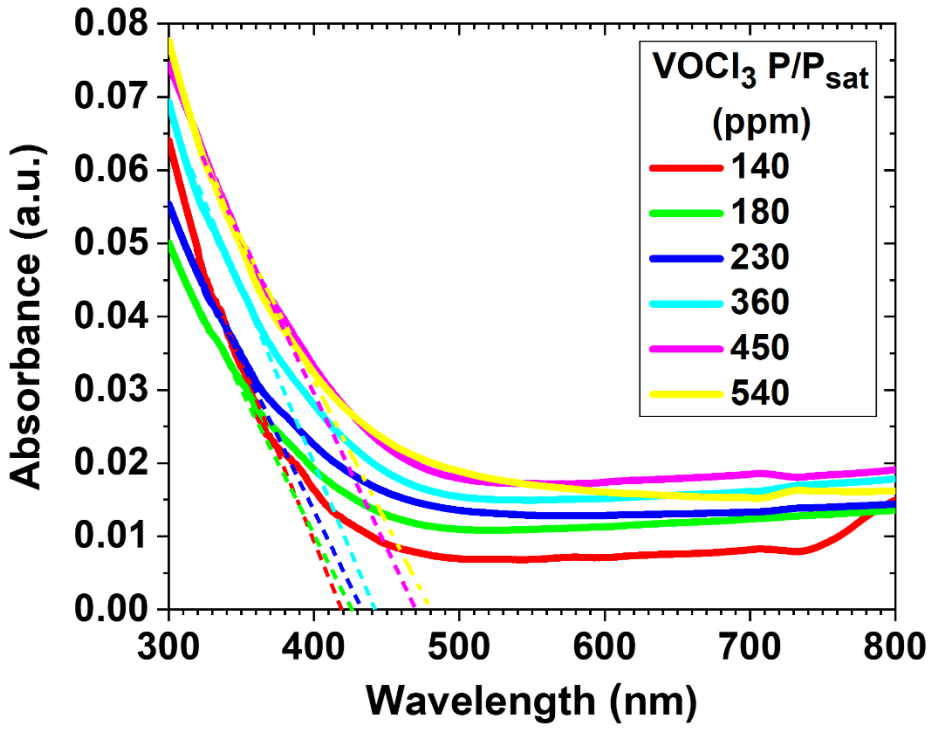

Fig. S6. The optical absorption spectra of PEDOT films. The effect of oxidant saturation ratio on the absorption wavelength (λ_{ab}) of films grown at the deposition temperature of 140 °C. The intersection of a line tangent to the absorption edge spectrum with the x-axis indicates the value of the absorption wavelength.

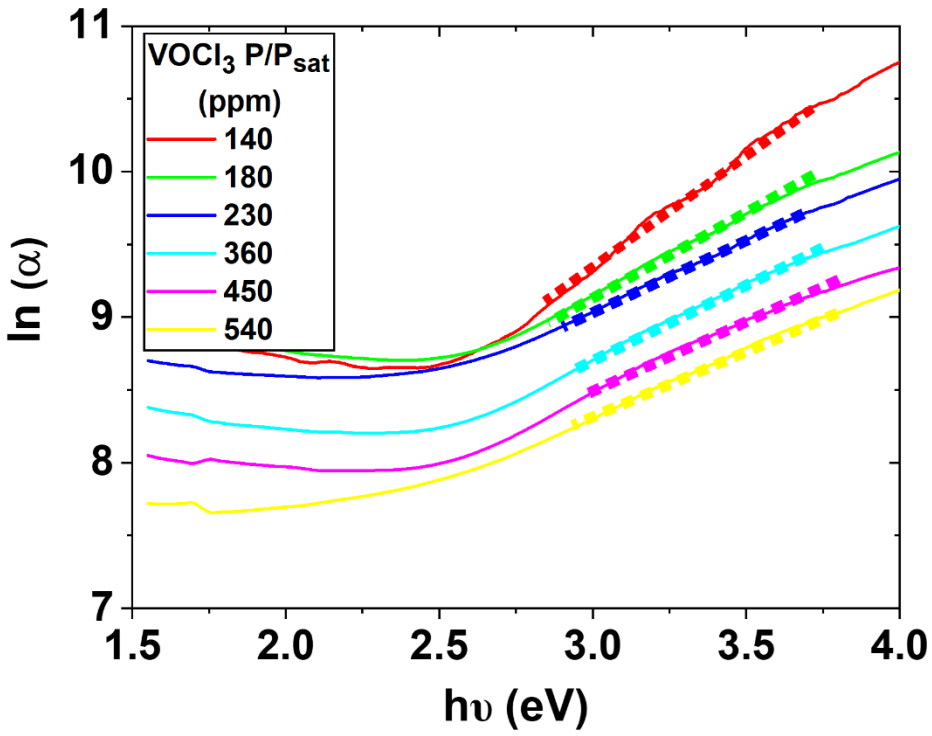

Fig. S7. Urbach plot for PEDOT films. The plot of $\ln(\alpha)$ versus incident photon energy for PEDOT films grown at the deposition temperature of 140 °C and different $VOCl_3$ saturation ratio. The inverse of slope beyond the optical band gap determines the Urbach energy (Eu).

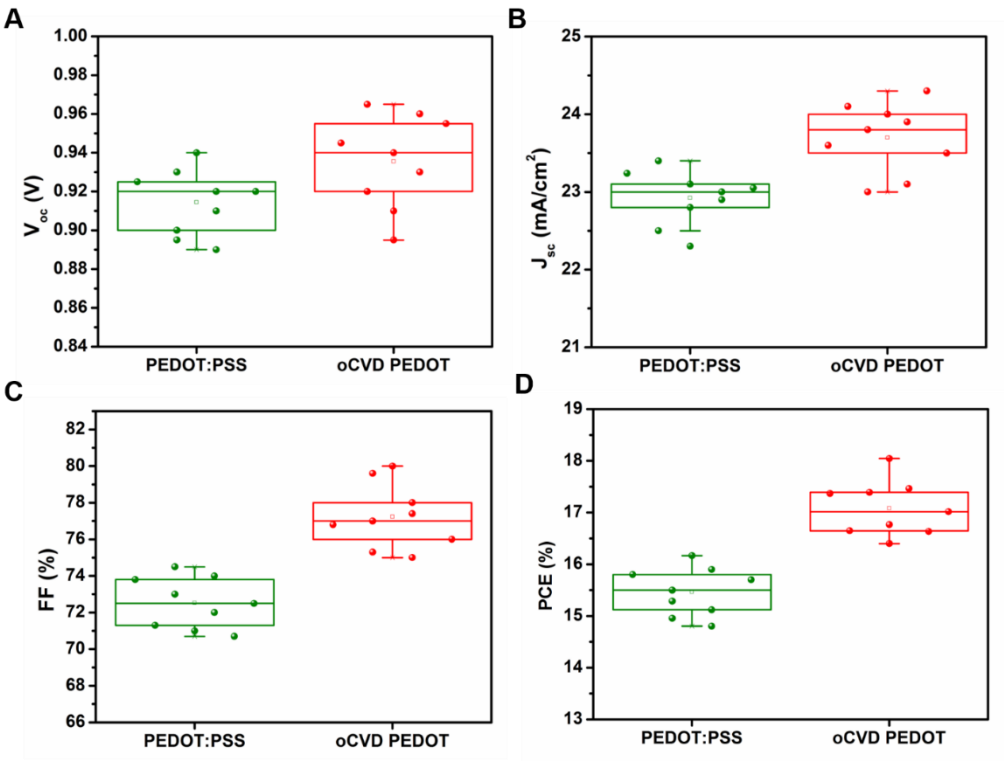

Fig. S8. Statistics of the PV parameters for the PSCs with different HTLs. The Statistics of the PSC devices based on PEDOT:PSS and oCVD PEDOT HTLs; (**A**) open circuit voltage (V_{oc}), (**B**) short circuit current density (J_{SC}), (**C**) fill factor (FF), and (**D**) power conversion efficiency (PCE).

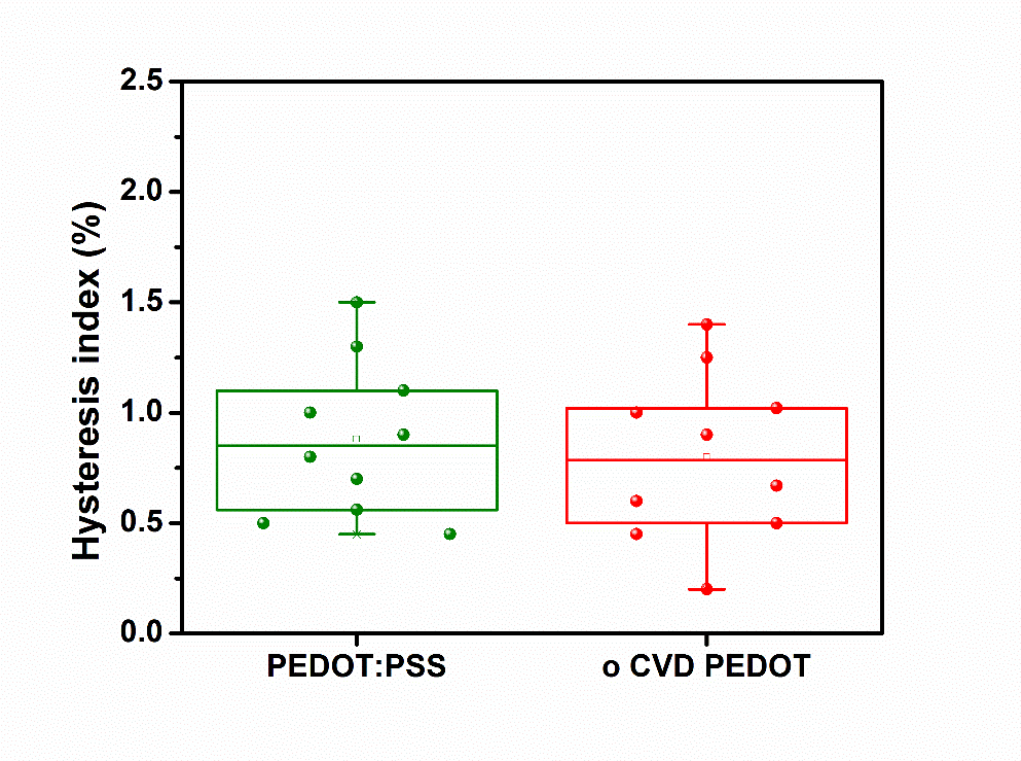

Fig. S9. Statistics of HIs for the PSC devices. The hysteresis indices of PSCs based on PEDOT:PSS and oCVD PEDOT HTLs. The values of the HIs were calculated from the following equation: $HI = ((PCE_{backward} - PCE_{forward})/PCE_{backward}) \times 100$.

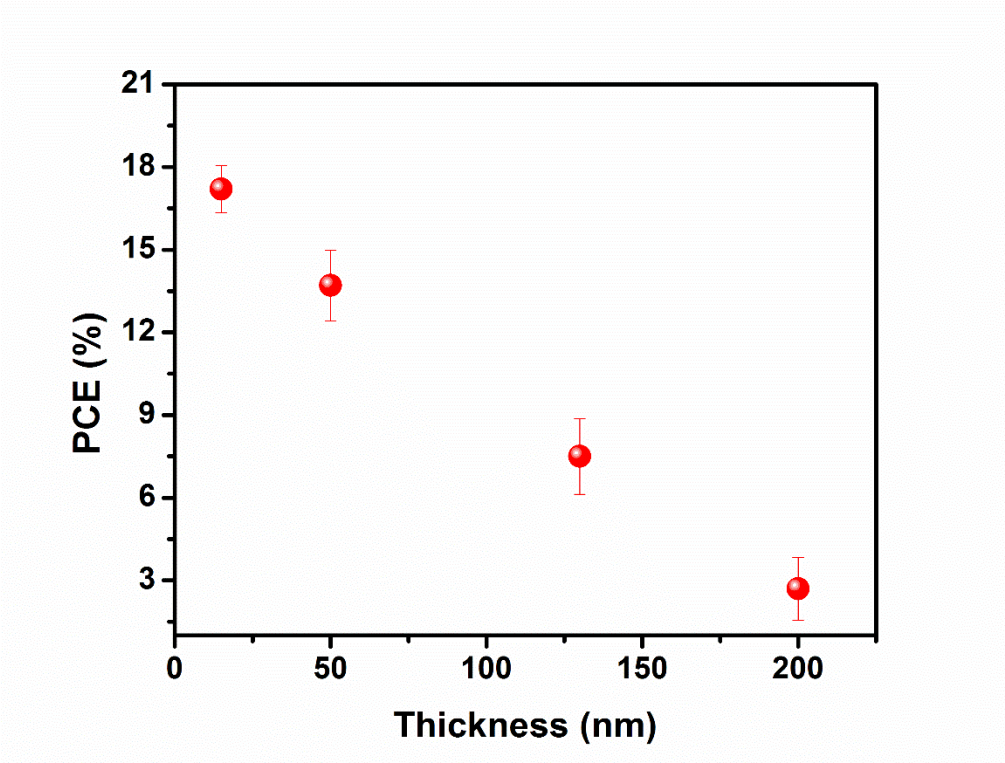

Fig. S10. Variation of PSC device performance versus the thickness of oCVD PEDOT. The effect of oCVD PEDOT film thickness on the PCE.